ELSEVIER

International Journal of Solids and Structures 41 (2004) 4927–4938

INTERNATIONAL JOURNAL OF SOLIDS and STRUCTURES

www.elsevier.com/locate/ijsolstr

Dynamic response of a projectile perforating multi-plate concrete targets

Shiqiao Gao, Lei Jin, Haipeng Liu *

School of Mechatronic Engineering, Beijing Institute of Technology, No. 5, Zhongguancun Nandajie, Haidia, Beijing 100081, PR China

Received 30 March 2004; received in revised form 30 March 2004
Available online 12 May 2004

Abstract

By means of the ultimate-density theory, the dynamic cavity-expansion theory and the stress-wave theory, the dynamic responses especially the deceleration curves of a projectile perforating multi-plates concrete targets are analyzed and calculated, the principles of scabbing on the rear surface of target plate are analyzed and illustrated. To verify the theoretical model, the deceleration tests are conducted for perforation of a projectile against multi-plates concrete targets by use of on-board recording system. Model predictions show good agreement with measurements from the tests.

Keywords: Projectile; Multi-plate target; Concrete; Penetration; Perforation; Scabbing; Dynamic response

1. Introduction

A multi-plates concrete target is composed of two or more parallel unreinforced concrete plates which have space intervals. Thus target can model the shelters, building structures, et al. To predict dynamic characteristic of a projectile impacting, penetrating, perforating and damaging a concrete target, the following three methods were proposed, improved and developed during the past 100 years (Backman and Goldsmith, 1978). They were empirical approach, analytical approach and numerical approach. In empirical approach (Bangush, 1993; Heuze, 1989), a series of empirical equations were given based on a lot of experiments and tests. But only some depth of penetration was obtained from the equations. They could not give us some dynamic characteristic curves versus time. In analytical approach, the cavity-expansion theory was developed and was considered as an effective method. But it could only deal with some cylindrical cavity or spherical cavity. It also neglected the time history effect of penetration. Numerical approach is widely used with the developments of modern computer techniques and finite element methods. But for concrete material penetrated by a projectile, the key techniques at present are not the computation techniques but the constitutive modeling techniques of damage.

* Corresponding author. Tel.: +86-1080695016; fax: +86-1068915087.
E-mail address: lhp@bit.edu.cn (H. Liu).

0020-7683/$ - see front matter © 2004 Elsevier Ltd. All rights reserved.
doi:10.1016/j.ijsolstr.2004.04.009

Because the time history curves of deceleration of a projectile play an important role in the designing of the projectile in particularly the fuze, we focus the study mainly on the curves of deceleration versus time.

For semi-infinite target, the penetrating projectile should stop in a definite depth whether its initial velocity is high or low. For a finite-thickness (slab) target especially for a thin target plate, if the striking velocity of projectile is high enough, in addition to penetration, perforation phenomenon will occur. Corresponding scabbing on the rear surface of target plate will be caused, which will reduce the real effective perforating thickness of the target plates.

In this paper, in terms of some phenomenon of experiments and tests, focusing on the time history process of penetration, firstly, a series of assumptions are presented and argued. Based on the theory of ultimate-density (Gao et al., 1994, 1995), the theory of cavity-expansion (Forrestal et al., 1996; Forrestal and Luk, 1998; Richard and Thomas, 2000; Young, 1998; Corbett et al., 1996), and the theory of shock wave, secondly, the analytical penetration equations are established which are derived from the mass conservation, momentum conservation and energy conservation. Finally, the dynamic responses especially the deceleration curves of a projectile are analyzed and calculated by means of computation and tests when it perforates a multi-plates concrete target.

2. Illustration of penetration and assumptions

The penetrating process of a projectile against concrete target is shown in Fig. 1 in which the coordinate $OXYZ$ describing the target and the coordinate $cr^*\beta z^*$ describing the projectile are given. The fractional space body (which is fan-shaped) $ABCD - A'B'C'D'$ of target is shown in Fig. 2. The face $ABCD$ is the same as the face of projectile, and the face $A'B'C'D'$ is the front of responding region.

The following assumptions are given and argued.

(1) The medium of concrete can be considered as ideal fluid for high-velocity impact, where the shear modulus is 0, which can satisfy the needs of engineering analysis for the case of high-velocity and high-pressure.

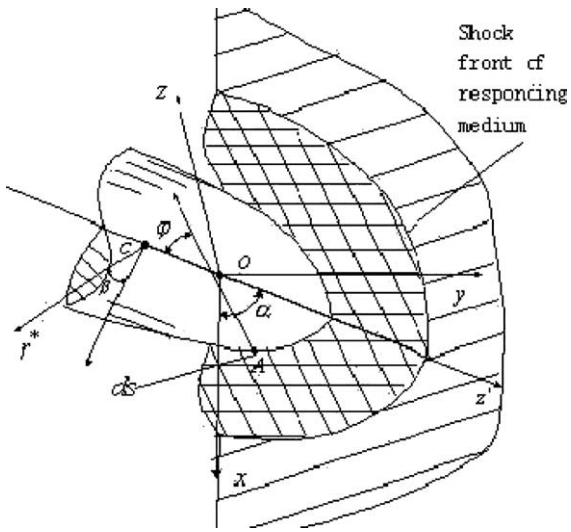

Fig. 1. The penetrating procedure of a projectile against concrete target.

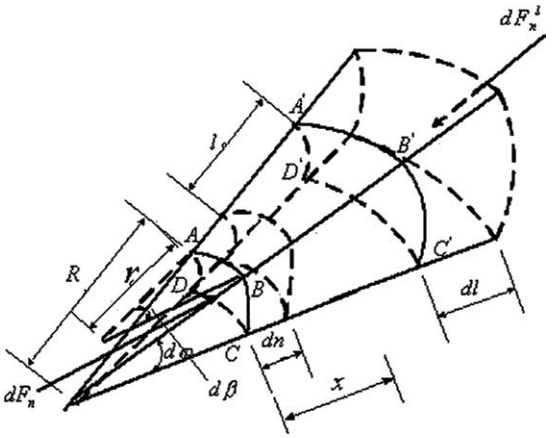

Fig. 2. The fractional space body $ABCD - A'B'C'D'$ of target.

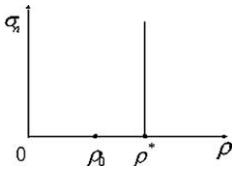

Fig. 3. The constitutive relation.

(2) To be compared with the compressive strength, the tensile strength is very little. For high-velocity and high-pressure impacting, the tensile strength can be neglected.
(3) During the impact or penetration, the elastic ultimate stress of concrete can be neglected while the wave velocity of elastic stress is very high.
(4) There is an ultimate density for concrete during the impact pressing, to which the density of concrete medium can not be increased again for further compressing, the constitutive relation can be seen from Fig. 3. A series of experiments had proved that the ultimate density had almost no changes for the higher pressure.
(5) During the compressing until ultimate density, the concrete medium subjects to ideal plastic deformation. There is no change of stress. In this process, the air voids are gradually compressed out of the concrete. The wave velocity of stress is 0.
(6) The region of medium response will expand in the external normal direction of the projectile surface.
(7) In the compressed region, the density and the volume of the concrete material have not any more changes. Therefore, the stress wave is constant-volume wave.
(8) The thermal conduction can be neglected during impacting.
(9) The projectile is non-deformable.

3. The dynamic penetration equations of the projectile

To derive the penetration equations, the mass conservation, the momentum conservation and energy conservation will be used during penetration.

3.1. The mass conservation

Considering that the total masses of responding medium of target in Fig. 2 are conservative, leads to

$$\int_0^{l+\mathrm{d}n} \rho^*(R+x)(r+x\sin\varphi)\,\mathrm{d}\beta\,\mathrm{d}\varphi\,\mathrm{d}x + \int_0^{\mathrm{d}l} \rho_0(R+l+x+\mathrm{d}n)[r+(l+\mathrm{d}n+x)\sin\varphi]\,\mathrm{d}\beta\,\mathrm{d}\varphi\,\mathrm{d}x = \int_{\mathrm{d}n}^{l+\mathrm{d}l+\mathrm{d}n} \rho^*(R+x)(r+x\sin\varphi)\,\mathrm{d}\beta\,\mathrm{d}\varphi\,\mathrm{d}x \tag{1}$$

whose form can also be written as

$$\rho^*\left[\int_{\mathrm{d}n}^{l+\mathrm{d}l+\mathrm{d}n} (R+x)(r+x\sin\varphi)\,\mathrm{d}\beta\,\mathrm{d}\varphi\,\mathrm{d}x - \int_0^{l+\mathrm{d}n} (R+x)(r+x\sin\varphi)\,\mathrm{d}\beta\,\mathrm{d}\varphi\,\mathrm{d}x\right] = \rho_0\int_0^{\mathrm{d}l} (R+l+x+\mathrm{d}n)[r+(l+\mathrm{d}n+x)\sin\varphi]\,\mathrm{d}\beta\,\mathrm{d}\varphi\,\mathrm{d}x$$

The other form is

$$\rho^*\left[\int_0^{\mathrm{d}l} (R+l+\mathrm{d}n+x)[r+(l+\mathrm{d}n+x)\sin\varphi]\,\mathrm{d}\beta\,\mathrm{d}\varphi\,\mathrm{d}x - \int_0^{\mathrm{d}n} (R+x)(r+x\sin\varphi)\,\mathrm{d}\beta\,\mathrm{d}\varphi\,\mathrm{d}x\right] = \rho_0\int_0^{\mathrm{d}l} (R+l+\mathrm{d}n+x)[r+(l+\mathrm{d}n+x)\sin\varphi]\,\mathrm{d}\beta\,\mathrm{d}\varphi\,\mathrm{d}x$$

By integrating the equation above, we get

$$\rho^*[(R+l)(r+l\sin\varphi)\,\mathrm{d}l\,\mathrm{d}\beta\,\mathrm{d}\varphi - Rr\,\mathrm{d}n\,\mathrm{d}\beta\,\mathrm{d}\varphi] = \rho_0(R+l)(r+l\sin\varphi)\,\mathrm{d}l\,\mathrm{d}\beta\,\mathrm{d}\varphi \tag{2}$$

which leads to:

$$\mathrm{d}l = \frac{\rho^*}{\rho^*-\rho_0}\cdot\frac{1}{\left(1+\frac{l}{R}\right)\left(1+\frac{l\sin\varphi}{r}\right)}\mathrm{d}n \tag{3}$$

We define a coefficient $k_1(l)$ as $k_1(l) = (1+\frac{l}{R})(1+\frac{l\sin\varphi}{r})$.

Noting that $c_n = \mathrm{d}l/\mathrm{d}t$, $v_n = \mathrm{d}n/\mathrm{d}t$, Eq. (3) can be written as

$$c_n = \frac{\rho^*}{\rho^*-\rho_0}\cdot\frac{1}{k_1(l)}v_n \tag{4}$$

where c_n is the wave velocity of responding medium, v_n is the particle velocity of the medium.

In this paper, the responding medium wave can be also called expansive wave. At the front of the expansive wave, from mass conservation we can obtain

$$\rho_0 c_n = \rho^*(c_n - v_n^l) \tag{5}$$

where v_n^l is the particle velocity at the front of responding medium wave.

Eq. (5) can be also written as

$$c_n = \frac{\rho^*}{\rho^*-\rho_0}\cdot v_n^l \tag{6}$$

Comparing Eq. (4) with Eq. (6), leads to

$$v_n^l = \frac{v_n}{k_1(l)} \tag{7}$$

It is known from Eq. (3) that, for plane wave, $k_1(l) \equiv 1$, the particle velocity is constant in the responding region; but for curve surface wave, $k_1(l) > 1$, the particle velocity is non-constant but varies in normal direction in the responding region. The distributing characteristic relation can be described as:

$$v_n^x = \frac{v_n}{k_1(x)} \quad (0 \leqslant x \leqslant l) \tag{8}$$

3.2. The momentum conservation

At the shock front, considering the momentum conservation, on the inner surface, there is

$$\mathrm{d}F_n^l = \rho_0 c_n v_n^l \cdot \mathrm{d}s' \tag{9}$$

where $\mathrm{d}F_n^l$ is the fractional force acting on the inner fractional front surface of expansive wave, $\mathrm{d}s'$ is the fractional area on the front of expansive wave.

It can be also written as

$$\sigma_n^l = \frac{\mathrm{d}F_n^l}{\mathrm{d}s'} = \rho_0 c_n v_n^l \tag{10}$$

Considering the momentum conservation of the fractional fan column $ABCD - A'B'C'D'$, the impulse of the external force $\mathrm{d}F_n$ in the time $\mathrm{d}t$ should be equal to the momentum change of $ABCD - A'B'C'D'$. The original momentum of the fractional fan column $ABCD - A'B'C'D'$ is

$$\mathrm{d}M = \int_0^{l+\mathrm{d}n} \rho^*(R+x)(r+x\sin\varphi)v_n^x \,\mathrm{d}x\,\mathrm{d}\beta\,\mathrm{d}\varphi$$

From Eq. (3) and omitting the higher order quantity, we get

$$\mathrm{d}M = \rho^* l v_n R r \,\mathrm{d}\beta\,\mathrm{d}\varphi \tag{11}$$

The momentum in the time interval $\mathrm{d}t$ is

$$\begin{aligned}\mathrm{d}M_{\mathrm{d}t} &= \int_0^{l+\mathrm{d}n} \rho^*(R+x)(r+x\sin\varphi)v_{n\,\mathrm{d}t}^x \,\mathrm{d}x\,\mathrm{d}\beta\,\mathrm{d}\varphi \\ &\quad + \int_0^{\mathrm{d}l} \rho_0(R+x+l+\mathrm{d}n)[r+(x+l+\mathrm{d}n)\sin\varphi]v_n^l \,\mathrm{d}x\,\mathrm{d}\beta\,\mathrm{d}\varphi \\ &= \rho^* \cdot l \cdot v_{n\,\mathrm{d}t} R r \,\mathrm{d}\beta\,\mathrm{d}\varphi + \rho_0 \cdot v_n \cdot \mathrm{d}l \cdot R r \,\mathrm{d}\beta\,\mathrm{d}\varphi \end{aligned} \tag{12}$$

By use of the momentum conservation, that is, the monument change $(\mathrm{d}M_{\mathrm{d}t} - \mathrm{d}M)$ equals to the impulse $\mathrm{d}F_n\,\mathrm{d}t$ in the time $\mathrm{d}t$, leads to

$$\mathrm{d}F_n\,\mathrm{d}t = \mathrm{d}M_{\mathrm{d}t} - \mathrm{d}M = (\rho^* l\,\mathrm{d}v_n + \rho_0 v_n\,\mathrm{d}l)R r\,\mathrm{d}\beta\,\mathrm{d}\varphi$$

Furthermore, there is

$$\mathrm{d}F_n = \left(\rho^* l \cdot \frac{\mathrm{d}v_n}{\mathrm{d}t} + \rho_0 v_n c_n\right)\mathrm{d}s \tag{13}$$

where $\mathrm{d}s = Rr \cdot \mathrm{d}\beta\,\mathrm{d}\varphi$ is the fractional area of the interface on the projectile surface whose relationship with $\mathrm{d}s'$ is $\mathrm{d}s' = k_1(l)\,\mathrm{d}s$.

From Eq. (13), we get

$$\sigma_n = \frac{\mathrm{d}F_n}{\mathrm{d}s} = \rho_0 c_n v_n + \rho^* l \cdot \frac{\mathrm{d}v_n}{\mathrm{d}t} \tag{14}$$

3.3. The energy conservation

We suppose that, the internal energy per unit mass is e, the fractional kinetic energy is $\mathrm{d}K$ and the fractional internal energy is $\mathrm{d}E$. By means of the energy conservation relationship during penetration, there is

$$\mathrm{d}F_n\,\mathrm{d}n = \mathrm{d}K + \mathrm{d}E \tag{15}$$

where

$$\begin{aligned}\mathrm{d}K &= \int_0^{l+\mathrm{d}n} \frac{1}{2}\rho^* k_1(x)[(v_{n\,\mathrm{d}t}^x)^2 - (v_n^x)^2]\,\mathrm{d}xRr\,\mathrm{d}\beta\,\mathrm{d}\varphi + \int_0^{\mathrm{d}l} \frac{1}{2}\rho_0 k_1(l+x)(v_n^x)^2\,\mathrm{d}xRr\,\mathrm{d}\beta\,\mathrm{d}\varphi \\ &= \rho^* v_n\,\mathrm{d}v_n lRr\,\mathrm{d}\beta\,\mathrm{d}\varphi + \frac{1}{2}\rho_0 k_1(l)v_n^l \cdot v_n^l\,\mathrm{d}l \cdot Rr \cdot \mathrm{d}\beta\,\mathrm{d}\varphi = \rho^* l v_n\,\mathrm{d}v_n\,\mathrm{d}s + \frac{1}{2}\rho_0 v_n v_n^l\,\mathrm{d}l\,\mathrm{d}s\end{aligned} \tag{16}$$

$$\mathrm{d}E = e \cdot \rho_0 \cdot \mathrm{d}l \cdot k_1(l)\,\mathrm{d}s \tag{17}$$

That is

$$\mathrm{d}F_n\,\mathrm{d}n = \rho^* l v_n\,\mathrm{d}v_n\,\mathrm{d}s + \tfrac{1}{2}\rho_0 v_n v_n^l\,\mathrm{d}l\,\mathrm{d}s + e \cdot \rho_0 \cdot \mathrm{d}l \cdot k_1(l)\,\mathrm{d}s \tag{18}$$

Noting that $\mathrm{d}n = v_n\,\mathrm{d}t$, $\sigma_n = \mathrm{d}F_n/\mathrm{d}s$, $\mathrm{d}l = c_n\,\mathrm{d}t$, leads to

$$\sigma_n = \rho^* l \cdot \frac{\mathrm{d}v_n}{\mathrm{d}t} + \frac{1}{2}\rho_0 c_n v_n^l + e \cdot \rho_0 \cdot \frac{c_n}{v_n^l} \tag{19}$$

By means of Eq. (14), we can obtain

$$\rho^* l \cdot \frac{\mathrm{d}v_n}{\mathrm{d}t} + \frac{1}{2}\rho_0 c_n v_n^l + e \cdot \rho_0 \frac{c_n}{v_n^l} = \rho^* l \cdot \frac{\mathrm{d}v_n}{\mathrm{d}t} + \rho_0 c_n v_n \tag{20}$$

Furthermore, the internal energy per unit mass can be written by

$$e = v_n^l\left(v_n - \frac{1}{2}v_n^l\right) = \left[k_1(l) - \frac{1}{2}\right](v_n^l)^2 \tag{21}$$

3.4. The penetration equations

Using the force applied on the nose of projectile derived above, considering the compressive strength σ_c and friction coefficient μ_f, for rigid projectile, by Newton's second law, in the direction of axis and in the direction of α-rotation, there are

$$\begin{cases} m\ddot{\xi} &= -\int\int_{s_A}(\mathrm{d}F_n + \sigma_c\,\mathrm{d}s)\cdot\cos\phi + (\mathrm{d}F_n + \sigma_c\,\mathrm{d}s)\cdot\mu_f\cdot\sin\phi \\ J_p\ddot{\alpha} &= \int\int_{s_A}[(\mathrm{d}F_n + \sigma_c\,\mathrm{d}s)(z^*\sin\phi - r^*\cos\phi) - \mu_f(\mathrm{d}F_n + \sigma_c\,\mathrm{d}s)(z^*\cos\phi + r^*\sin\phi)]\cos\beta\,\mathrm{d}s \end{cases} \tag{22}$$

Substituting Eq. (13) into Eq. (22), leads to

$$\begin{cases} (m_p + m_f)\ddot{\xi} &= -\iint_{s_A}\left[\frac{\rho^*\rho_0}{\rho^* - \rho_0}\cdot\frac{v_n^2}{k_1(l)} + \sigma_c\right](\cos\varphi + \mu_f\sin\varphi)\,\mathrm{d}s \\ J_p\ddot{\alpha} &= \iint_{s_A}\left\{\left[\frac{\rho^*\rho_0}{\rho^* - \rho_0}\cdot\frac{v_n^2}{k_1(l)} + \sigma_c\right] + \rho^* l\ddot{\xi}\cos\varphi\right\}\cdot[(z^*\sin\varphi - r^*\cos\varphi) \\ & \quad -\mu_f(z^*\cos\varphi + r^*\sin\varphi)]\cos\beta\,\mathrm{d}s \end{cases} \tag{23}$$

where m_p is the mass of projectile, and $m_f = \iint_{s_A}\rho^* l(\cos\varphi + \mu_f\sin\varphi)\cos\varphi\,\mathrm{d}s$ is adjunctive mass, σ_c is static compressive strength, J_p is the moment of inertia of the projectile relative to axes r^*, μ_f is dynamic friction

coefficient, the others parameters are shown in Fig. 1. The variable $\ddot{\xi}$ is tangent acceleration of the centroid trajectory of the projectile and its direction is identical with the projectile axes z^*, $\dot{\alpha}$ is angular velocity of the projectile relative to axes r^*.

The relationship between the normal velocity v_n and axial velocity v_ξ and angular velocity $\dot{\alpha}$ is

$$v_n = v_\xi \cos\varphi + \dot{\alpha}(z^* \sin\varphi - r^* \cos\varphi)\cos\beta \tag{24}$$

4. The characteristic equation of scabbing

4.1. Wave propagation during penetration

According to the analysis and assumption mentioned above, the fastest wave is elastic wave during penetration, then is compressed responding medium wave (or expansive wave) and finally is constant-volume wave in compressed medium. The elastic wave velocity is $c_e = \sqrt{E/\rho_0}$. The velocity of expansive wave c_n is given by Eq. (4). The velocity of constant-volume wave in compressed medium is $c_v = \sqrt{E/[2(1+\mu)\rho^*]}$. All of their propagation characteristic curves are shown in Fig. 4.

The velocity of compressed responding medium wave c_n is not constant. Its characteristic relation is not linear but non-linear. Its value depends on instantaneous velocity v_n and expanding displacement l. Integrating Eq. (4), we get

$$k_2(l)l = \frac{\rho^*}{\rho^* - \rho_0}\int_0^t v_n \,\mathrm{d}t \tag{25}$$

where $k_2(l) = 1 + \frac{1}{2}\left(\frac{1}{R} + \frac{\sin\varphi}{r}\right)l + \frac{l^2\sin\varphi}{3Rr}$.

This equation is the characteristic curves shown in Fig. 4. Fig. 4 shows also the state of stress wave related to the time t_1 and t_2.

4.2. The stress criterion of scabbing

In this paper, we consider that, the scabbing is caused by the reflection of attenuation wave on the free surface. After reflection of stress wave on free surface, the original compress wave will change to tensile wave. When the tensile stress wave meets with the compressed stress wave, their values will be added. When the resultant stress is greater than the tensile strength of the material, once crack will be caused. We suppose that the tensile stress of concrete is σ_s, there is

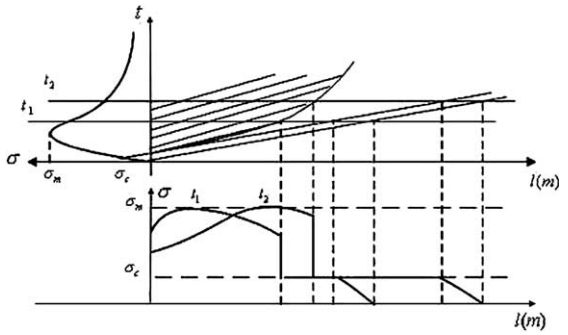

Fig. 4. Wave propagation during penetration.

$$\sigma^* - \sigma \geqslant \sigma_s \tag{26}$$

where σ^* is the front peak value of the attenuation stress wave, σ is the compressing stress where crack is caused.

4.3. The dimension criterion of scabbing

4.3.1. The total scabbing

Eq. (26) is the stress criterion of scabbing for each time. As mentioned above, the total scabbing is composed of the scabbing from all the times. The accumulative dimension criterion should be

$$s + l = 2H \tag{27}$$

where s is the penetration depth of the projectile, l is the propagation displacement of stress wave at the same time, H is the thickness of target. They are all shown in Fig. 5. By means of Eq. (25), we can obtain the displacement of the stress wave in the time of t. The penetration depth s can be described as

$$s = \int_0^t v_n \Big|_{\varphi=0} \mathrm{d}t \tag{28}$$

That is

$$k_2(l)l|_{\varphi=0} = \frac{\rho^*}{\rho^* - \rho_0} s \tag{29}$$

Substituting Eq. (29) into Eq. (27), leads to

$$k_2(l)l|_{\varphi=0} \frac{\rho^* - \rho_0}{\rho^*} + l = 2H \tag{30}$$

The scabbing thickness h shown in Fig. 5 is

$$h = l - H \tag{31}$$

Substituting Eq. (30) into Eq. (31), leads to

$$h = \frac{l}{2}\left[1 - k_2(l)|_{\varphi=0} \frac{\rho^* - \rho_0}{\rho^*}\right] \tag{32}$$

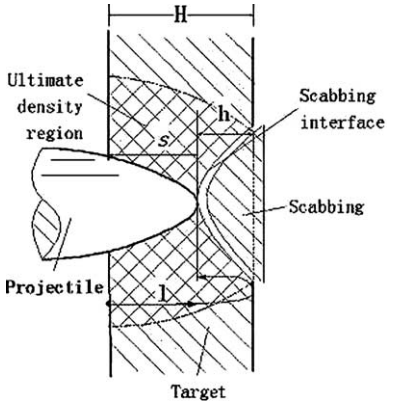

Fig. 5. The stress-wave echo and scabbing.

4.3.2. Scabbing for each time

The approximate analysis of the stress criterion of scabbing for each time is as follows.

From the point of view of analytical approach, by means of Eq. (10) and in axial direction ($\varphi = 0$), taking v as the function of the instant penetration depth x, we can obtain

$$\sigma(x) = \frac{\sigma(0)}{v^2(0)} v^2(x) \tag{33}$$

If we set $\sigma_{\max} = \sigma(0)$, and $v^2(0) = v_0^2$, from Eq. (10), we get

$$\sigma_{\max} = \sigma(0) = \frac{\rho_0 \rho^*}{\rho^* - \rho_0} v_0^2 \tag{34}$$

Thus, Eq. (26) can be written as:

$$\sigma(0) - \sigma(2h) \geqslant \sigma_s \tag{35}$$

That is

$$\frac{\rho_0 \rho^*}{\rho^* - \rho_0} (v_0^2 - v^2(2h)) \geqslant \sigma_s \tag{36}$$

Solving it, we get

$$h \geqslant h(v_0, \sigma_s) \tag{37}$$

Substantially, the total thickness of scabbing $\sum h$ cut down the effective thickness of the target to be subject to penetration.

5. The impacting experiments and calculations for multi-plates targets

Just as the former statement, the projectile will perforate the target if the velocity is enough high for a finite-thickness target. Simultaneously, the projectile will perforate a multi-plates target when it has enough high velocity and energy. To study effectively, in addition to theoretic analysis, a series of tests on the perforating of a projectile against a multi-plates target was conducted.

5.1. The test scheme and design

In order to record the striking load effectively, in the tests, we choose the on-board storage system and the accelerator which can record high G striking load. Accelerator is piezoelectricity film sensor which can be subjected to a high load. The storage system is RAM. Fig. 6 shows the measurement system diagram.

The working principle of this system is as follows. Before the experiment, turn on the power. The measuring system will begin circularly sampling according to the initialized cycle. Before the projectile contacting with the target, the system will keep in a state of circularly sampling because the striking

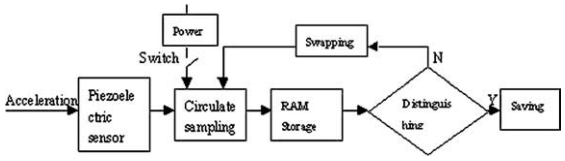

Fig. 6. Measurement system diagram.

acceleration and its voltage are lower than the preset one. When the projectile contacting with the target, the system will stop circularly sampling and reach to the final state of recording and storing, because the striking acceleration increasing suddenly. The data in storage are read and dealt with by computer in an effective time. We can also reappear measuring information.

5.2. The numerical calculation

Eq. (23) is non-linear differential equation that has no simple analytical resolution. The control differential equation will be resolved iteratively through the central deference method. The essential central deference equations are

$$\begin{cases} \left.\dfrac{\mathrm{d}^2x}{\mathrm{d}t^2}\right|_{x_{i+1}} = \dfrac{x_{i+2} - 2x_{i+1} + x_i}{(\Delta t)^2} \\ \left.\dfrac{\mathrm{d}x}{\mathrm{d}t}\right|_{x_{i+1}} = \dfrac{x_{i+2} - x_{i+1}}{\Delta t} \end{cases} \tag{38}$$

The curve surface integral stated in Eq. (23) will be made by Gauss's six points integral method.

6. The results from calculations and tests and their comparison

By means of the method given above, the tests and calculations are made on the deceleration characteristics of parabola-nose projectile perpendicularly penetrating into multi-plates concrete targets. The geometric equation of parabola nose of projectile is

$$z^* = 0.11\left(1 - \frac{r^{*2}}{0.025^2}\right) + 0.065 \quad (r^* \leqslant 0.025)$$

The density of concrete is $\rho = 2400$ kg/m^3; the ultimate density is $\rho^* = 2640$ kg/m^3, the compressive strength $\sigma_c = 3.0 \times 10^7$ N/m^2; the mass of the projectile $m_p = 7.63$ kg; the moment of inertia $J_p = 0.162$ kg/m^2; the friction coefficient $\mu_f = 0.1$; the thickness of single target plate is 0.3 m.

Two tests for different original striking velocities and different amounts of concrete plats are conducted. In the first test, the multi-plates target consists of two concrete plates between which the distance is 1 m, and the original striking velocity of the projectile is 532 m/s. In the second test, the target includes three concrete plates whose interval distance are also 1 m, and the original striking velocity of the projectile is 580 m/s. Fig. 7 shows the perforation and the scabbing in a perforated concrete target plates. Fig. 8 shows the perforated concrete target plates in the second test.

The deceleration curves of the projectile from measurement in the first test and corresponding analytical calculation are shown in Fig. 9. The deceleration curves of the projectile from measurement in the second test and corresponding analytical calculation are given in Fig. 10. From the curves in Fig. 9, it can be seen that, at the time of 0.45 ms, the target has been perforated and has lost resistance. The corresponding penetration depth (which can be also called effective thickness of concrete plate) at this moment is only 0.18 m, but not the original thickness 0.3 m. The reason is from the scabbing. Such a phenomenon can been also seen from the curves in Fig. 10 for the second test. From the results of tests and calculations comparison for both tests, it is known that, the results from analytical analyses are in good agreement with those from tests.

Fig. 7. The perforation and scabbing of a perforated concrete target plate.

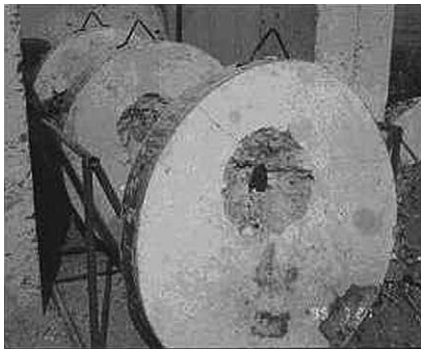

Fig. 8. The perforated concrete plates in the second group test.

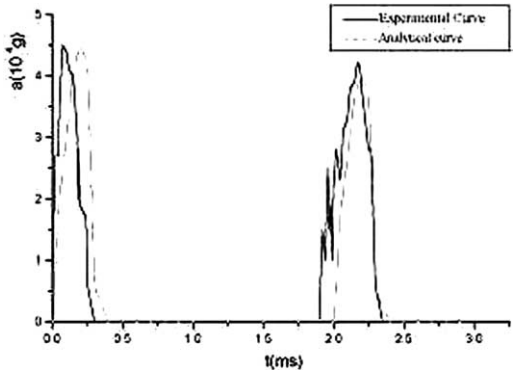

Fig. 9. The measurement and calculation deceleration curves of a projectile in the first test.

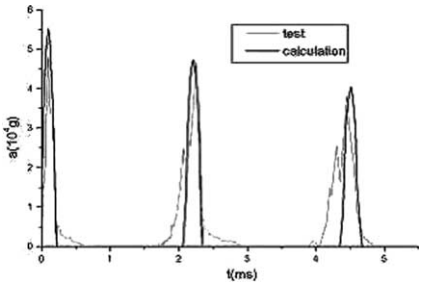

Fig. 10. The measurement and calculation deceleration curves of a projectile in the second test.

7. Conclusion

We developed an analysis model that predicted deceleration of a rigid projectile penetrating multi-plate concrete targets. Based on the theory of propagation and reflection of stress waves, we presented an analytical method to calculate scabbing on the rear of target plate. The results were in good agreement with those data from filed tests and verified the methods and models presented in the paper.

References

Backman, M.E., Goldsmith, W., 1978. The mechanics of projectiles into targets. Int. J. Engng. Sci. 16, 1–99.

Bangush, M.Y.H., 1993. Formula for non-deformable missiles impacting on concrete targets. In: Impact and Explosion. CRC Press, Boca Raton, FL, pp. 370–380.

Corbett, G.G., Reid, S.R., Johnson, W., 1996. Impact loading of plates and shells by free-flying projectiles. Int. J. Impact Engng. 18, 144–230.

Forrestal, M.S., Luk, V.K., 1998. Dynamic spherical cavity-expansion in a compressible elastic–plastic solid. J. Appl. Mech. 55, 275–279.

Forrestal, M.S., Frew, D.J., Hanchak, S.J., Brar, N.S., 1996. Penetration of grout and concrete targets with ogive-nose steel projectiles. Int. J. Impact Engng. 18, 465–476.

Gao, S., Shi, G., Tan, H., Guo, Z., 1994. Dynamic analysis of projectile-fuze system impacting half-infinite concrete target with small fall-angle. J. Beijing Inst. Technol. 14 (4), 359–365.

Gao, S., Liu, M., Tan, H., 1995. Dynamic analysis of penetrator into half-infinite concrete target. ACTA Amarmenterii 16 (4), 46–50.

Heuze, F.E., 1989. An overview of projectile penetration into geological material, with emphasis on rocks. In: Schwer, L.E., Salamon, N.J., Liu, W.K. (Eds.), Computational Techniques for Contact, Impact, Penetration and Perforation of Solids. American Society of Mechanical Engineering (ASME), New York, pp. 275–308.

Richard, W.M., Thomas, A.D., 2000. Finite cavity expansion method for near-surface effects and layering during earth penetration. Int. J. Impact Engng. 24, 239–258.

Young, C.N., 1998. Simplified analytical model of penetration with lateral, loading-user's guide. SAND98-0978. Sandia National Laboratory, Albuquerque, NM.